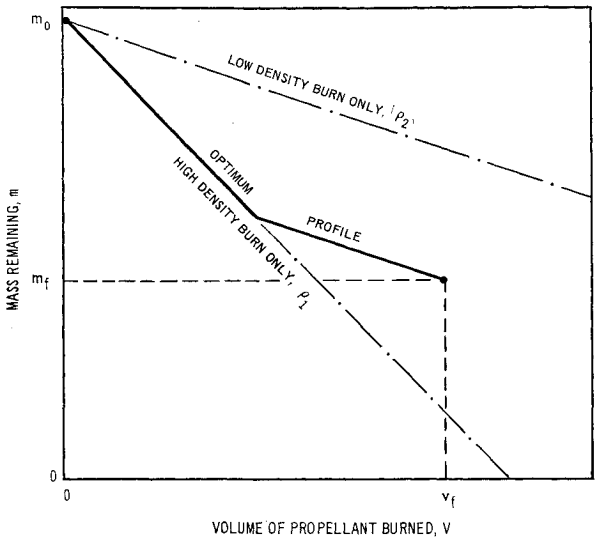

Fig. 1 Mass remaining vs volume of propellant burned.

It has been noted by Leitmann[3] that the application of optimal control theory to this problem will also yield an optimum solution. Results indicate that the optimum burn profile is sequential with the higher density mode preceding. It should be stressed, however, that the control found in this manner is extremal only and its optimality can be established by invoking existence or sufficiency theorems, or by recourse to direct reasoning as in the preceding paragraph.

Conclusion

To maximize ideal Δv for a two-mode one-stage rocket, the optimum burn profile is purely sequential, with the higher density mode operating first.

References

[1] Salkeld, R., "Mixed-mode Propulsion for the Space Shuttle," *Astronautics and Aeronautics*, Vol. 9, No. 8, 1971, pp. 52–58.

[2] Leitmann, G., "On the Equation of Rocket Motion," *Journal of British Interplanetary Society*, July–Sept. 1957, 16(3), pp. 141–147.

[3] Leitmann, G., private communication, Nov. 3, 1971, System Development Corp., Santa Monica, Calif.

Effects of Heat Addition in Divergent Nozzles with Application to MPD Thrusters

M. SAJBEN* AND G. E. CHMIELEWSKI†
McDonnell Douglas Research Laboratories, McDonnell Douglas Corporation, St. Louis, Mo.

A WIDE variety of MPD thruster configurations have been described in the literature, many of which have a recognizable area minimum or geometrical throat. Electrode arrangement varies greatly among the various designs, so that the bulk of the (usually large) electromagnetic energy input to the propellant gas can occur either upstream or downstream of the geometric throat. A large part of the total energy input is in the form of ohmic heating which influences the gas-dynamic contribution to the total thrust. The purpose of this Note is to point out that heat addition, when applied downstream of the geometric throat, can lead to unusual gas-dynamic behavior including the presence of shocks. In comparison, heating upstream of the throat produces no unexpected features.

These findings follow from the steady, one-dimensional gas-dynamic equations neglecting friction but taking area change and heat addition into account. The energy equation is represented by a simple specification of total temperature along the nozzle axis. Assumption of thermodynamic equilibrium, the perfect gas relation $p = \rho RT$, and the definition of total temperature in terms of Mach number results in a closed set of equations for ρ, p, T, T_0 and v.

The equation governing $M(x)$ can be written[1] as a function of distance along the axis (as measured from the throat):

$$\frac{dM^2}{dx} = 2M^2\left(1 + \frac{\gamma - 1}{2} M^2\right) \times \frac{\frac{1}{2}(1 + \gamma M^2)(1/T_0)dT_0/dx - (1/A)dA/dx}{1 - M^2} \quad (1)$$

where $T_0(x)$ and $A(x)$ are assumed to be known functions. Note that the actual independent variable is the area A since x could be cancelled out. (The scale of the x variable is consequently arbitrary, but it will be retained for convenience.)

Equation (1) may have more singular points than the one familiar from the classic adiabatic nozzle case. They occur if $M = 1$ and the following condition is satisfied:

$$(1/A)\, dA/dx = [(1 + \gamma)/2]\, (1/T_0)\, dT_0/dx \quad (2)$$

For demonstration purposes, we consider the example of an axially symmetric nozzle with a hyperbolic contour

$$R/R_* = [1 + \{(x/R_*) \tan \theta\}^2]^{1/2} \quad (3)$$

where θ is the asymptotic half-cone angle for the nozzle and R_* is the throat radius. The total temperature is described arbitrarily by:

$$\frac{T_0(x)}{T_{01}} = 1 + \frac{1}{2}(\tau - 1)\left\{1 + \tanh\left[\left(\frac{x - \bar{x}}{R_*}\right)\left(\frac{R_*}{\lambda}\right)\right]\right\} \quad (4)$$

where $\bar{x}$ is the location of the maximum in heating rate dT_0/dx, and λ is the characteristic axial distance of the heating zone. $\tau \equiv T_{02}/T_{01}$ is the ratio of total temperatures across the zone.

Closer examination shows that, in this example, Eq. (2) may be satisfied at any number of points from none to three depending on the value of the total temperature ratio. The absence of singularities corresponds to fully subsonic flow. One singular point will occur if τ is either less than 2.2 or more than 18 (approximately). In the first case the singular point occurs very near the throat, in the second case it is located a short distance downstream of the heating zone. Three singular points will occur if $2.2 \lesssim \tau \lesssim 18$. Two singular points represent intermediate, degenerate situations corresponding to either $\tau \simeq 2.2$ or $\tau \simeq 18$.

Figure 1 shows the nozzle contour defined by Eq. (3) and the total temperature and heating rate distributions defined by Eq. (4). The curves shown correspond to $\theta = 45°$, $\bar{x}/R_* = 2$, $R_*/\lambda = 2$ and $\tau = 4$. Figure 2 shows a family of $M(x)$ solutions for argon ($\gamma = \frac{5}{3}$) with τ as the parameter, obtained through the numerical integration of Eq. (1). In each curve, the integration was started at the appropriate singular point, where the derivative was evaluated analytically. Depending on the value of τ, the solutions may be grouped into three qualitatively different types.

The first type corresponds to $1.0 \leq \tau \lesssim 2.2$ and one singular

Received November 22, 1971; revision received February 17, 1972. This research was conducted under the McDonnell Douglas Independent Research and Development Program.

Index categories: Nozzle and Channel Flow; Electric and Advanced Space Propulsion.

* Associate Scientist. Member AIAA.

† Research Scientist.

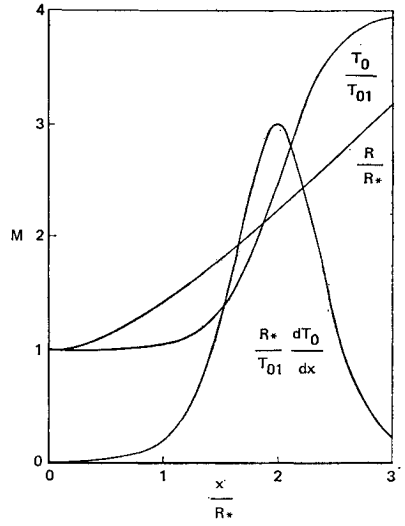

Fig. 1 Nozzle shape and distribution of total temperature and its derivative along the axis.

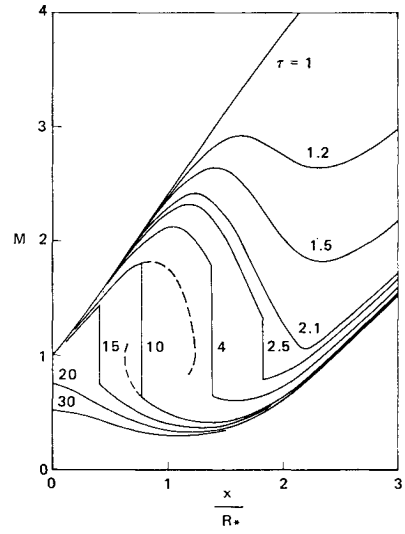

Fig. 2 Numerically computed $M(x)$ solutions with $\tau = T_{02}/T_{01}$ as the parameter.

point near the throat. The flow is completely supersonic past the choking point, although the Mach number is greatly reduced across the heating zone, as expected.

The second type of solution occurs if $2.2 \lesssim \tau \lesssim 18$, i.e., if three singular points exist. It is found that the solution which passes from subsonic to supersonic flow at the first singular point cannot be extended to the nozzle exit; it does not have real values above some maximum x/R_* and is therefore physically meaningless. Conversely, the solution passing through the third singular point has no meaning below a certain x/R_*. The actual shape of the integral curves is illustrated by dotted lines on Fig. 2 (for the case of $\tau = 10$ only). A physically meaningful solution connecting subsonic plenum with supersonic exit conditions can be constructed only by incorporating a normal shock in the pattern. The location of the shock is determined by requiring that the normal shock relation be satisfied between the two Mach numbers. Solutions of this type display two choking points, i.e., two locations at which the Mach number is unity.

Further increases in total temperature cause the shock to move upstream until it reaches the geometric throat at $\tau \simeq 18$. Increases in heating above this value establish a third type of solution, corresponding to one singular point (choking point), located just downstream of the heating zone, at $x/R_* \simeq 2.45$. The flow is subsonic throughout most of the nozzle including the geometric throat. It appears that a sufficiently large increase of total temperature, if accomplished within a sufficiently short distance, can switch the choking point from the geometric throat to a new position well downstream of it.

It is clear that there exists a design pressure ratio for each value of τ and that the nozzle can operate in either an overexpanded or an underexpanded condition, in the same way as an adiabatic nozzle. If the exit pressure is kept constant at the design value for an adiabatic nozzle, then the addition of heat will result in increasingly overexpanded operation, which in turn involves a certain penalty in thrust.

The consequences of the described behavior in terms of the externally observable performance variables of the nozzle are shown in Fig. 3. The variables are: $\tilde{v} = v/(RT_{01})^{1/2}$, $\tilde{W} = W(RT_{01})^{1/2}/(A_* p_{01})$ and $\tilde{F} = F/(A_* p_{01})$, representing the variation of exit velocity v, mass flow rate W and net thrust or gasdynamic force F. (This thrust clearly does not include electromagnetic contributions.) Numerical computations were made for the τ values indicated by circles, the continuous line represents an interpolation.

The thrust values plotted are maxima, obtained by the appropriate design pressure ratio for each τ. Continuous lines refer to heat added downstream of the throat, while dotted lines indicate the results of adding the same amount of heat in the plenum. The latter case is rather straightforward since $\tilde{v} \sim (T_{02})^{1/2}$, $\tilde{W} \sim 1/(T_{02})^{1/2}$, and $\tilde{F} = \text{const}$. Figure 3 clearly shows that adding heat in the plenum chamber increases the exit velocity and thereby the specific impulse, reduces mass flow, but does not influence thrust. In contrast, adding moderate amounts of heat in the divergent portion of the nozzle does not change the mass flow but increases thrust through increasing the exit velocity. (In this respect, the situation here is somewhat analogous to the operation of afterburners in jet engines.) If the heat addition is extreme ($\tau > 18$ in the present example), then the velocity in the geometric throat becomes subsonic and the mass flow is correspondingly reduced, as indicated by the break in the $\tilde{W}$ curve of Fig. 3. This reduction of mass flow outweighs the effects of increasing velocity, and the thrust drops slightly for $\tau > 18$.

The present calculations have some rather obvious limitations: nonequilibrium, three-dimensional, viscous and electromagnetic effects may mask or overwhelm the features discussed herein. Nevertheless there may be designs or ranges of

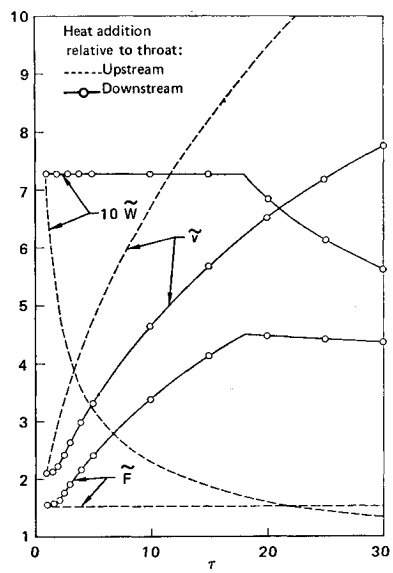

Fig. 3 Variation of normalized mass flow ($\tilde{W}$), normalized exit velocity ($\tilde{V}$), and normalized thrust ($\tilde{F}$) as functions of τ.

operating conditions where these purely gasdynamic considerations could explain experimental findings.

Finally, the authors wish to raise the question of stability of solutions which exhibit two choking points separated by a shock. A situation of this sort may well be found unstable, in which case the present study may be relevant to fluctuations observed in some thrusters.

Reference

[1] Shapiro, A. H., *The Dynamics and Thermodynamics of Compressible Fluid Flow*, Vol. 1, Ronald Press, New York, 1953, p. 230.

Recursive Filter Initialization

RICHARD H. BATTIN,* STEVEN R. CROOPNICK,† AND JAMES M. HABBE‡
Charles Stark Draper Laboratory, Cambridge, Mass.

THE application of recursive filtering techniques to space navigation requires that the associated state vector and error covariance matrix be specified both initially and at those times when reinitialization of the filter is required to cope with problems of divergence and instability. A fairly common initialization method, and one that is used in Apollo navigation,[1] is to postulate that the initial errors in the state are uncorrelated and spherically distributed, which implies that the initial covariance matrix of estimation errors is diagonal. The true state vector errors are, of course, correlated and several measurements must be processed before the covariance matrix begins to exhibit proper cross-correlations.

The purpose of this Note is to describe an initialization technique which partially accounts for these correlations, considerably reduces the undesirable transient effects of the first few measurements, and acts to inhibit filter divergence when the interval between measurements is inordinately large. The improvement in navigation performance is quite dramatically illustrated (in the second of the two examples considered below) for a space shuttle vehicle navigating with the aid of somewhat sparsely distributed ground beacons.

The method consists of including in the initial covariance matrix the effect of a number of pseudo-measurements of certain orbital parameters. Specifically, define the measurement geometry vector $\mathbf{b}$ to represent, to a first order of approximation, the variation in the measured quantity Q which would result from variations in the components of the state vector $\mathbf{x}$. That is

$$\mathbf{b} = (\partial Q/\partial \mathbf{x})^T \tag{1}$$

By identifying Q with an orbital parameter expressed in terms of the components of the state vector and calculating the necessary partial derivatives, the measurement geometry vector $\mathbf{b}$ may be determined from the initial estimate of the state. Although no direct measurement of the parameter is made, this measurement information can be adjoined to the error covariance matrix by assuming a reasonable value for a measurement variance and updating the covariance matrix as though an actual measurement had been performed.

Two orbital parameters that have proved to be particularly useful for this purpose are the total energy

$$E = v^2/2 - \mu/r \tag{2}$$

and the angular momentum

$$h = |\mathbf{h}| = |\mathbf{r} \times \mathbf{v}| \tag{3}$$

Assuming the state vector to be six-dimensional

$$\mathbf{x}^T = (\mathbf{r}^T, \mathbf{v}^T) \tag{4}$$

the corresponding geometry vectors $\mathbf{b}_E$ and $\mathbf{b}_h$ are readily obtained from Eq. (1) as

$$\mathbf{b}_E = \begin{pmatrix} \mu\mathbf{r}/r^3 \\ \mathbf{v} \end{pmatrix} \tag{5}$$

$$\mathbf{b}_h = (1/h)\begin{pmatrix} \mathbf{v} \times \mathbf{h} \\ \mathbf{h} \times \mathbf{r} \end{pmatrix} \tag{6}$$

This technique was applied[2] to the problem of navigating a spacecraft during the midcourse phase of a moon-to-Earth flight. A desired or nominal trajectory for the trans-Earth path was assumed known and the vehicle given the necessary position and velocity to achieve this trajectory with the exception of small initial position and velocity perturbations at the time of the trans-Earth insertion from the back side of the moon. The measurements of the state consisted of angles

Table 1 Cislunar simulation parameters and standard deviations

Parameter	Value used in the filter model	Value used to simulate actual environment
rms error in μ_E	0	1.24×10^7 miles^3/hr^2
rms error in μ_M	0	1.52×10^5 miles^3/hr^2
rms error in Earth axes	0.2 miles	0.2 miles
rms error in moon radius	0.2 miles	0.5 miles
rms Earth horizon error	1.2 miles	6.2 miles
rms moon horizon error	0.9 miles	1.9 miles
Sextant rms error	5.0×10^{-5} rad	7.4×10^{-5} rad
Sextant bias	0	4.16×10^{-5} rad

Standard deviation of angular momentum pseudo-measurement = 25 miles^2/hr
Standard deviation of energy pseudo-measurement = 9.439×10^4 (miles/hr)^2
Initial (diagonal) position standard deviations = 5.68 miles
Initial (diagonal) velocity standard deviations = 20.45 miles/hr

Received February 18, 1972; revision received March 6, 1972. This research was partially supported by Manned Spacecraft Center contract NAS 9-4065 T. O. 41.

Index categories: Navigation, Control, and Guidance Theory; Spacecraft Navigation Guidance, and Flight-Path Control Systems.

* Associate Director, Charles Stark Draper Laboratory. Fellow AIAA.

† Staff Scientist, Charles Stark Draper Laboratory. Associate Member AIAA.

‡ Research performed while Master's degree candiate at MIT, currently at Naval Avionics Facility, Indianapolis, Indiana.